

Experimental Cerenkov luminescence tomography of the mouse model with SPECT imaging validation

Zhenhua Hu,¹ Jimin Liang,¹ Weidong Yang,² Weiwei Fan,³ Congye Li,³ Xiaowei Ma,² Xueli Chen,¹ Xiaopeng Ma,¹ Xiangsi Li,¹ Xiaochao Qu,¹ Jing Wang,^{2,*} Feng Cao,^{3,*} and Jie Tian^{1,4,*}

¹Life Sciences Research Center, School of Life Sciences and Technology, Xidian University, Xi'an, 710071, China

²Department of Nuclear Medicine, Xijing Hospital, Fourth Military Medical University, Xi'an 710032, China

³Department of Cardiology, Xijing Hospital, Fourth Military Medical University, Xi'an 710032, China

⁴Institute of Automation, Chinese Academy of Sciences, Beijing 100190, China

*tian@ieee.org

Abstract: Optical molecular imaging resulting from Cerenkov radiation has become a motivating topic recently and will potentially open new avenues for the study of small animal imaging. Cerenkov-based optical imaging taken from living animals *in vivo* has been studied with two-dimensional (2D) planar geometry and three-dimensional (3D) homogeneous mouse model. In this study, we performed 3D Cerenkov-based luminescence tomography (CLT) using a heterogeneous mouse model with an implanted Na¹³¹I radioactive source, which provided the accurate location for the reconstructed source. Furthermore, single photon emission computed tomography (SPECT) was utilized to verify the results of 3D CLT. We reconstructed the localization and intensity of an embedded radioactive source with various concentrations, and established a quantitative relationship between the radiotracer activity and the reconstructed intensity. The results showed the ability of *in vivo* CLT to recover the radioactive probe distribution in the heterogeneous mouse model and the potential of a SPECT imaging validation strategy to verify the results of optical molecular tomography.

©2010 Optical Society of America

OCIS codes: (170.3880) Medical and biological imaging; (110.6960) Tomography; (260.3800) Luminescence; (170.2655) Functional monitoring and imaging; (170.3660) Light propagation in tissues.

References and links

1. R. Weissleder, and M. J. Pittet, "Imaging in the era of molecular oncology," *Nature* **452**(7187), 580–589 (2008).
2. R. Weissleder, and V. Ntziachristos, "Shedding light onto live molecular targets," *Nat. Med.* **9**(1), 123–128 (2003).
3. V. Ntziachristos, J. Ripoll, L. V. Wang, and R. Weissleder, "Looking and listening to light: the evolution of whole-body photonic imaging," *Nat. Biotechnol.* **23**(3), 313–320 (2005).
4. V. Ntziachristos, C. H. Tung, C. Bremer, and R. Weissleder, "Fluorescence molecular tomography resolves protease activity *in vivo*," *Nat. Med.* **8**(7), 757–761 (2002).
5. W. Cong, G. Wang, D. Kumar, Y. Liu, M. Jiang, L. Wang, E. Hoffman, G. McLennan, P. McCray, J. Zabner, and A. Cong, "Practical reconstruction method for bioluminescence tomography," *Opt. Express* **13**(18), 6756–6771 (2005), <http://www.opticsinfobase.org/abstract.cfm?URI=OPEX-13-18-6756>.
6. Y. Lv, J. Tian, W. Cong, G. Wang, J. Luo, W. Yang, and H. Li, "A multilevel adaptive finite element algorithm for bioluminescence tomography," *Opt. Express* **14**(18), 8211–8223 (2006), <http://www.opticsinfobase.org/abstract.cfm?URI=oe-14-18-8211>.
7. H. Dehghani, S. C. Davis, S. Jiang, B. W. Pogue, K. D. Paulsen, and M. S. Patterson, "Spectrally resolved bioluminescence optical tomography," *Opt. Lett.* **31**(3), 365–367 (2006), <http://www.opticsinfobase.org/abstract.cfm?URI=ol-31-3-365>.
8. X. Song, D. Wang, N. Chen, J. Bai, and H. Wang, "Reconstruction for free-space fluorescence tomography using a novel hybrid adaptive finite element algorithm," *Opt. Express* **15**(26), 18300–18317 (2007), <http://www.opticsinfobase.org/VJBO/viewmedia.cfm?uri=oe-15-26-18300&seq=0>.

9. J. Tian, J. Bai, X. P. Yan, S. Bao, Y. Li, W. Liang, and X. Yang, "Multimodality molecular imaging," *IEEE Eng. Med. Biol. Mag.* **27**(5), 48–57 (2008).
10. A. Joshi, J. C. Rasmussen, E. M. Sevick-Muraca, T. A. Wareing, and J. McGhee, "Radiative transport-based frequency-domain fluorescence tomography," *Phys. Med. Biol.* **53**(8), 2069–2088 (2008).
11. R. Han, J. Liang, X. Qu, Y. Hou, N. Ren, J. Mao, and J. Tian, "A source reconstruction algorithm based on adaptive *hp*-FEM for bioluminescence tomography," *Opt. Express* **17**(17), 14481–14494 (2009), <http://www.opticsinfobase.org/abstract.cfm?URI=oe-17-17-14481>.
12. Y. Lin, W. C. Barber, J. S. Iwanczyk, W. Roeck, O. Nalcioglu, and G. Gulsen, "Quantitative fluorescence tomography using a combined tri-modality FT/DOT/XCT system," *Opt. Express* **18**(8), 7835–7850 (2010), <http://www.opticsinfobase.org/abstract.cfm?URI=oe-18-8-7835>.
13. G. Wang, W. Cong, K. Durairaj, X. Qian, H. Shen, P. Sinn, E. Hoffman, G. McLennan, and M. Henry, "*In vivo* mouse studies with bioluminescence tomography," *Opt. Express* **14**(17), 7801–7809 (2006), <http://www.opticsinfobase.org/abstract.cfm?URI=OE-14-17-7801>.
14. Y. Lu, H. B. Machado, Q. Bao, D. Stout, H. Herschman, and A. F. Chatziioannou, "*In vivo* mouse bioluminescence tomography with radionuclide-based imaging validation," *Mol. Imaging. Biol.* (2010).
15. R. Robertson, M. S. Germanos, C. Li, G. S. Mitchell, S. R. Cherry, and M. D. Silva, "Optical imaging of Cerenkov light generation from positron-emitting radiotracers," *Phys. Med. Biol.* **54**(16), N355–N365 (2009).
16. F. Boschi, A. E. Spinelli, D. D'Ambrosio, L. Calderan, M. Marengo, and A. Sbarbati, "Combined optical and single photon emission imaging: preliminary results," *Phys. Med. Biol.* **54**(23), L57–L62 (2009).
17. H. Liu, G. Ren, Z. Miao, X. Zhang, X. Tang, P. Han, S. S. Gambhir, Z. Cheng, and A. Boswell, "Molecular optical imaging with radioactive probes," *PLoS ONE* **5**(3), e9470 (2010).
18. A. E. Spinelli, D. D'Ambrosio, L. Calderan, M. Marengo, A. Sbarbati, and F. Boschi, "Cerenkov radiation allows *in vivo* optical imaging of positron emitting radiotracers," *Phys. Med. Biol.* **55**(2), 483–495 (2010).
19. C. Li, G. S. Mitchell, and S. R. Cherry, "Cerenkov luminescence tomography for small-animal imaging," *Opt. Lett.* **35**(7), 1109–1111 (2010), <http://www.opticsinfobase.org/abstract.cfm?uri=ol-35-7-1109>.
20. J. V. Jelley, "Cerenkov radiation and its applications," *Br. J. Appl. Phys.* **6**(7), 227–232 (1955).
21. M. Schweiger, S. R. Arridge, M. Hiraoka, and D. T. Delpy, "The finite element method for the propagation of light in scattering media: boundary and source conditions," *Med. Phys.* **22**(11), 1779–1792 (1995).
22. G. Wang, Y. Li, and M. Jiang, "Uniqueness theorems in bioluminescence tomography," *Med. Phys.* **31**(8), 2289–2299 (2004).
23. P. E. Gill, W. Murray, and M. Wright, *Practical Optimization*, (Academic Press, New York, 1981).
24. J. S. Cho, R. Taschereau, S. Olma, K. Liu, Y. C. Chen, C. K. Shen, R. M. van Dam, and A. F. Chatziioannou, "Cerenkov radiation imaging as a method for quantitative measurements of beta particles in a microfluidic chip," *Phys. Med. Biol.* **54**(22), 6757–6771 (2009).
25. X. Chen, X. Gao, D. Chen, X. Ma, X. Zhao, M. Shen, X. Li, X. Qu, J. Liang, J. Ripoll, and J. Tian, "3D reconstruction of light flux distribution on arbitrary surfaces from 2D multi-photographic images," *Opt. Express* **18**(19), 19876–19893 (2010), <http://www.opticsinfobase.org/abstract.cfm?URI=oe-18-19-19876>.
26. G. Alexandrakis, F. R. Rannou, and A. F. Chatziioannou, "Tomographic bioluminescence imaging by use of a combined optical-PET (OPET) system: a computer simulation feasibility study," *Phys. Med. Biol.* **50**(17), 4225–4241 (2005).
27. J. E. Bowsler, V. E. Johnson, T. G. Turkington, R. J. Jaszczak, C. R. Floyd, and R. E. Coleman, "Bayesian reconstruction and use of anatomical *a priori* information for emission tomography," *IEEE Trans. Med. Imaging* **15**(5), 673–686 (1996).

1. Introduction

Molecular imaging has become an essential tool for the biomedical imaging field in recent years, and a variety of imaging systems have been widely used in preclinical and clinical applications [1]. These systems include computed tomography (CT), magnetic resonance imaging (MRI), positron emission tomography (PET), single photon emission computed tomography (SPECT), and ultrasound. New imaging technologies, especially optical imaging technologies, are increasingly being used for earlier diagnosis of diseases and for discovery and evaluation of new drugs [2,3].

Among the optical imaging technologies, fluorescence and bioluminescence imaging are rapidly gaining popularity because they can reflect molecular specificity [2]. Presently, *in vivo* optical imaging of living animals is mainly two-dimensional (2D) planar imaging. The lack of depth information in 2D images might limit its further development. Three-dimensional (3D) optical tomography overcomes this limitation and provides a more precise spatial distribution of probes by using an accurate photon migration theory and relevant mathematical models [2,3]. Many studies have shown that 3D spatial distribution of the probes can be reconstructed [4–12]. However, the effectiveness and accuracy of these algorithms remain to be validated. Dissection is one of the verification strategies, which usually damages the biological tissues and only provides an approximate position of the light

source. An *in vivo* CT imaging strategy was also used to validate artificial source-based optical experiments [13,14]. If the reconstruction results of optical tomography can be validated by other imaging technologies, such as PET or SPECT, it will be more robust.

Recently, novel research emerged in *in vivo* optical imaging of small living animals based on Cerenkov radiation [15–19]. Cerenkov radiation is a well-known phenomenon in which visible and near-infrared photons are emitted when a charged and high-energy particle travels faster than the speed of light in a dielectric medium [20]. Robertson *et al.* first presented *in vivo* optical imaging of the Cerenkov light emitted from positron-emitting radiotracers [15]. Liu *et al.* successfully demonstrated that a variety of radionuclides can be imaged with an optical imaging instrument [17]. Li *et al.* presented Cerenkov luminescence tomography (CLT) for small-animal imaging [19]. However, the positron-emitting radiotracer activity distribution was reconstructed based on a homogeneous mouse model. In this study, we performed *in vivo* 3D CLT based on a heterogeneous mouse model. In addition, a SPECT imaging validation strategy was also proposed to verify the results of 3D CLT. We reconstructed the localization and intensity of an embedded radioactive source with various concentrations, and preliminarily established a quantitative relationship between the radiotracer activity and the reconstructed intensity.

2. Methods

Photon propagation in biological tissues can be accurately modeled by the radiative transport equation (RTE). However, solving RTE is quite complicated and time-consuming. Under the diffusion condition which requires the dominance of scattering over absorption, the first order approximation of RTE, called the diffusion equation (DE), provides acceptable accuracy with decreased computational cost. Cerenkov photon migration in tissues can be described by the steady-state DE [21].

Based on DE, an adaptive *hp*-finite element method (*hp*-FEM) for bioluminescence source reconstruction proposed by our research group [11] is employed in this paper to recover the Cerenkov light source distribution. Based on this algorithm, the relationship between the Cerenkov light source and surface flux density can be established as follows:

$$A_k S_k^P = \Phi_k^C \quad (1)$$

where A_k is the system matrix for the k -th level mesh; S_k^P is the Cerenkov light source distribution located in the permissible source region that is determined by *a priori* knowledge and Φ_k^C is the nodal flux density on the surface.

Because of the ill-posed nature of the internal source reconstruction [22], it is difficult to solve Eq. (1) directly. The classical Tikhonov regularization method can be employed to solve Eq. (1). The following optimization problem is defined to determine the Cerenkov light source distribution:

$$\min_{S_{\inf} \leq S_k^P \leq S_{\sup}} \Theta(S_k^P) = \|A_k S_k^P - \Phi_k^C\|_{L^2(\Omega)} + \lambda_k \|S_k^P\|_{L^2(\Omega)} \quad (2)$$

where S_{\inf} and S_{\sup} are the lower and upper bounds of the Cerenkov light source power density and λ_k denotes the regularization parameter. $L^2(\Omega)$ is the weight matrix and satisfies $\|V\|_{L^2(\Omega)} = V^T L^2(\Omega) V$. This minimization problem is solved by a modified Newton method with an active set strategy [23].

3. Experiments and results

3.1 *In vitro* imaging experiment of $Na^{131}I$

A series of *in vitro* experiments were designed and conducted to study the characteristics of the emitted light from $Na^{131}I$. First, radioactive sources with various activities were imaged

for acquiring optical signals. The radioactive sources ($n = 6$) were made of glass vessels that were filled with Na^{131}I . The dimensions of the sources were approximately 3.42 mm in diameter and 7 mm in length. The activities of the radioactive sources were 100 μCi , 200 μCi , 300 μCi , 400 μCi , 500 μCi and 600 μCi respectively. A control source was filled with a non-radioactive NaI solution. All of them were imaged for 3 minutes with the Xenogen In Vivo Imaging System (IVIS Kinetic, Caliper Life Sciences) as shown in Fig. 1(a). Luminescence was quantified in units of photons per second per square centimeter per steradian ($P \cdot s^{-1} \cdot \text{cm}^{-2} \cdot \text{sr}^{-1}$). From Fig. 1(a), we found that the radioactive sources emitted a mass of light, but the signal detected in the control source was non-existent. The optical signal proportionally increased with increasing activity.

An experiment that aimed to estimate the spectral characteristics of emitted light during ^{131}I decay was then performed. The above radioactive sources were imaged using the standard filter set installed on the IVIS system including 515-575 nm (GFP), 575-650 nm (DsRED), 695-770 nm (Cy5.5) and 810-875 nm (ICG). The measured spectrum presented a broad and continuous distribution from 500 nm to 900 nm, and the spectrum distribution of the emitted-light from the radioactive source with an activity of 300 μCi is shown in Fig. 1(b). The broad spectrum suggested that the produced light was correlated with Cerenkov radiation [24]. Since many types of biological tissues in the near-infrared region (650-900 nm) satisfy the diffusion condition, Cerenkov photon migration in tissues can be described by DE with acceptable accuracy.

To study the connection between the emitted optical signal and nuclear signal from the radioactive sources, the foregoing radioactive sources were imaged with the SPECT-CT system (Symbia T2, Siemens). Regions of interest (ROIs) were drawn, and the counts per pixel were converted to counts per pixel per second. ROIs were also drawn over the optical images of the six radioactive sources, and the average radiances were read by Living Image 3.2 software (IVIS Kinetic, Caliper Life Sciences). The average radiances provided the intensities of the optical signals. The intensities of optical and nuclear signals as a function of activity are depicted in Fig. 2(a). We found that both of the signals increased linearly with increasing activity. Moreover, there was a robust correlation between the activity versus the optical ($r^2 = 0.982$) and nuclear signals ($r^2 = 0.997$), as well as the optical signal versus the nuclear signal ($r^2 = 0.98$) (Fig. 2(a)-(b)).

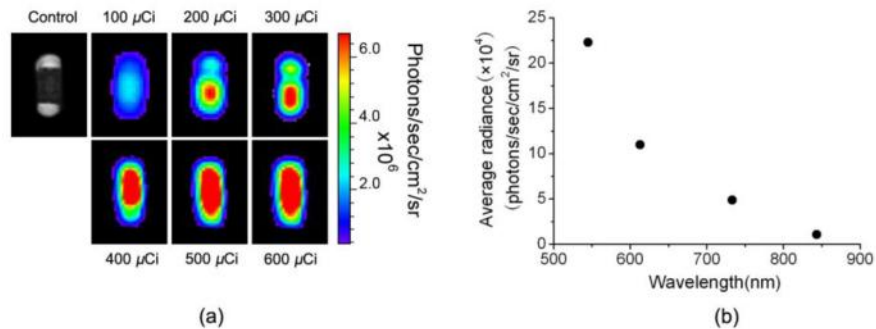


Fig. 1. Radioactive sources imaging. (a) Fusion of luminescent image and the corresponding photograph of the control source and radioactive sources respectively. The activities of the radioactive sources were 100 μCi , 200 μCi , 300 μCi , 400 μCi , 500 μCi and 600 μCi respectively. (b) Spectrum distribution of the emitted-light from the radioactive source with an activity of 300 μCi .

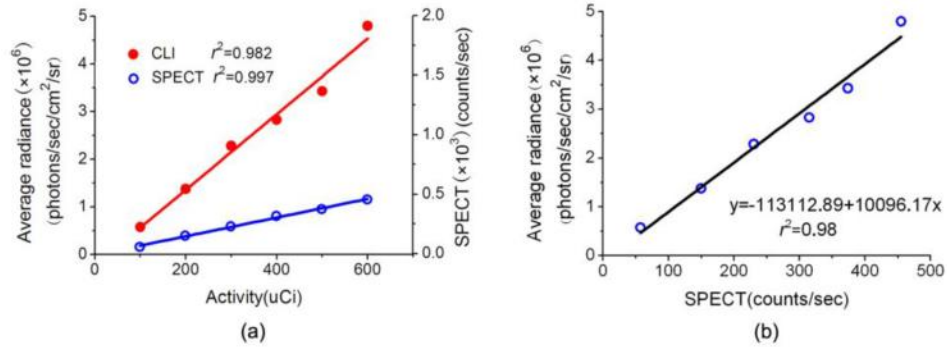


Fig. 2. Correlation analysis between Cerenkov luminescence imaging (CLI) and SPECT imaging. (a) Quantification of imaging signals showed a drastic increase from 100 μ Ci to 600 μ Ci. (b) Quantification of signals showed a robust *in vitro* correlation between CLI and SPECT imaging ($r^2 = 0.98$).

3.2 *In vivo* 3D CLT based on a heterogeneous mouse model

To perform *in vivo* 3D CLT of an electron-emitting radiotracer based on a heterogeneous animal model, an adult athymic nude mouse with an implanted Na¹³¹I radioactive source was imaged with a dual-modality ZKKS-Direct3D molecular imaging system (jointly developed by Guangzhou Zhongke Kaisheng Medical Technology CO., Ltd, Xidian University and Institute of Automation, CAS). This system is comprised of an optical imaging system and a micro-CT system. The central piece of the system is an animal-imaging holder which is used to affix the anesthetized mouse. The optical imaging system employs a scientific liquid-cooled back illuminated CCD camera (Princeton Instruments PIXIS 2048B, Roper Scientific, Trenton, NJ) coupled with an imaging lens (Nikon Normal Macro 55 mm $f/2.8$). The CCD camera generates 2048×2048 16-bit images with a $13.5 \mu\text{m} \times 13.5 \mu\text{m}$ pixel size. The micro-CT system consists of a micro-focus X-ray source (Oxford Instruments Series5000 Apogee, CA) with a $35 \mu\text{m}$ focal spot size, a tuning range of 4 to 50 kVp voltage, and 0 to 1.0 mA current; along with an X-ray detector (HAMAMATSU C7921CA-02, Hamamatsu, Japan) with a voltage detection range from 20 to 100 kVp with a $50 \mu\text{m} \times 50 \mu\text{m}$ pixel size.

In the experiment, an adult male athymic nude mouse underwent aseptic celiotomy. The animal received isoflurane (2%) for general anesthesia. A radioactive source made of a glass vessel that was filled with approximately 600 μ Ci Na¹³¹I was implanted in the abdomen. The radioactive source was dipped in alcohol for <20 min for antiseptis before implantation. All animal procedures were in accordance with the Fourth Military Medical University (FMMU) approved animal protocol. After implantation, the mouse was affixed to the animal-imaging holder and placed on the rotation stage. The rotation stage was vertically rotated under computer control for acquisition of multi-view luminescent images and micro-CT projection data. Luminescent images were acquired using a 675-775 nm filter with a binning value of 4, integration time of 5 min and aperture number $f_{num} = 8$. Figure 3(a)-(d) shows the four luminescent images superimposed on the corresponding photographs in the anterior-posterior, left lateral, right lateral, and posterior-anterior views respectively. For acquiring structural information from biological tissues, the mouse was scanned by the micro-CT system in the vertical position immediately after celiac administration of the contrast material iohexol using the following imaging parameters: 40 kVp, 700 μ A, and a 5 min scan.

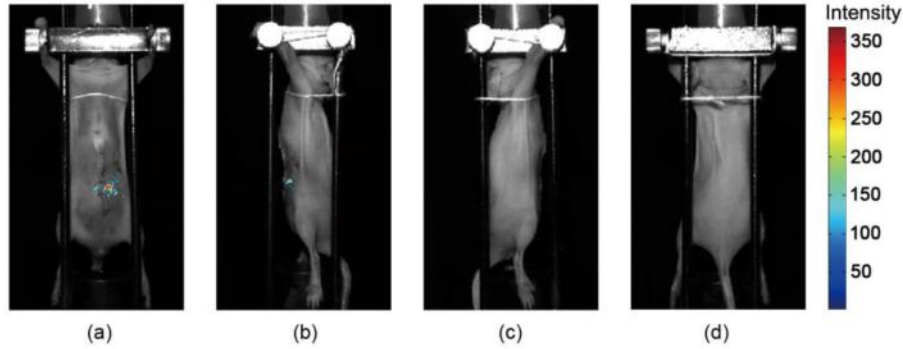


Fig. 3. Luminescent views in pseudo-color superimposed on the corresponding photographs of the mouse with an implanted $600 \mu\text{Ci}$ Na^{131}I radioactive source. (a)-(d) Anterior-posterior, left lateral, right lateral, and posterior-anterior views respectively.

Reconstructed CT images were segmented into several major anatomical components including adipose, heart, lungs, liver, stomach, and kidneys. A geometrical model of the mouse was generated consisting of 26640 tetrahedral elements and 4980 nodes as shown in Fig. 4(a). The acquired 2D luminescence images on the CCD camera were mapped onto the 3D mesh surface of the geometrical model using the method proposed in [25] as shown in Fig. 4(b). Based on the light flux distribution on the surface, an initial permissible source region was selected as $\Omega = \{(x, y, z) | 17 < x < 27, 20 < y < 29, 4 < z < 16\}$. Optical parameters of biological tissues at wavelengths of 675-775 nm were calculated based on literature [26].

Using the adaptive *hp*-FEM algorithm [11], the 3D distribution information of an internal Na^{131}I radioactive source was reconstructed as shown in Fig. 5(a). In order to analyze the results quantitatively, we defined the distance error $d = \sqrt{(x - x_0)^2 + (y - y_0)^2 + (z - z_0)^2}$, where (x, y, z) was the coordinate of the reconstructed source with maximum density, and (x_0, y_0, z_0) was that of the actual source. The position of the actual source could be obtained by the micro-CT images as (24.80, 21.90, 9.30) mm, and the location of the reconstructed source was (23.17, 20.50, 9.23) mm. The distance error was 2.15 mm. In addition, we performed CLT based on a homogeneous mouse model. A 3D rendering of the reconstructed source distribution in the homogeneous mouse model is shown in Fig. 5(b). The distance error between the actual source and the reconstructed one was 4.41 mm. Comparison of the reconstruction results based on the heterogeneous and homogeneous mouse models are listed in Table 1, which demonstrates that the reconstruction results based on the heterogeneous mouse model are more accurate in localization than the homogeneous one. Figure 5(c) shows the micro-CT slice fused with the reconstructed source (red triangle) based on the heterogeneous mouse model from a sagittal view. We also found that the reconstructed source based on the heterogeneous mouse model was very close to the location of the implanted source (inside the black circle). Our data showed the ability of *in vivo* CLT to recover the radioactive probe distribution in a heterogeneous mouse model.

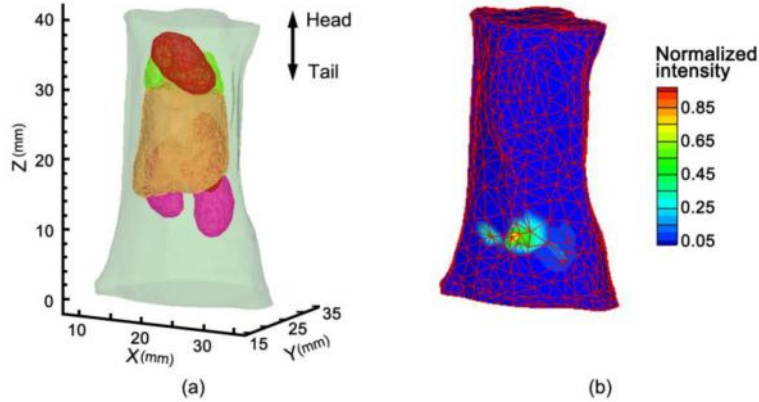


Fig. 4. Mouse model with an implanted $600 \mu\text{Ci Na}^{131}\text{I}$ radioactive source and its associated luminescent measurement. (a) A geometrical model of the mouse chest consisting of adipose, heart, lungs, liver, stomach, and kidneys. (b) The measured luminescent data mapped onto the 3D mesh surface of the mouse chest.

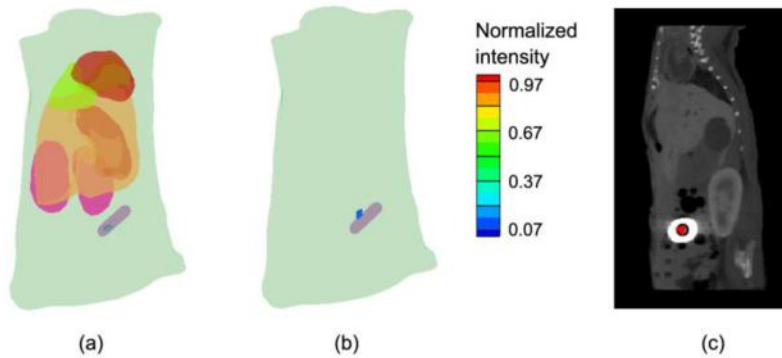


Fig. 5. CLT reconstruction of the radioactive source distribution in the mouse with an implanted $600 \mu\text{Ci Na}^{131}\text{I}$ radioactive source. (a) and (b) are the 3D renderings of the reconstructed source distribution in heterogeneous and homogeneous mouse models respectively. (c) The true source (inside the black circle) in a micro-CT slice superimposed with the reconstructed source (red triangle) from a sagittal view.

Table 1. Comparison of reconstruction results based on heterogeneous and homogeneous mouse models

Mouse model	Actual source center (mm)	CLT reconstructed location (mm)	d (mm)
Homogeneous	(24.80, 21.90, 9.30)	(20.83, 20.46, 10.58)	4.41
Heterogeneous	(24.80, 21.90, 9.30)	(23.17, 20.50, 9.23)	2.15

3.3 SPECT imaging validation experiment

In the previous section, we recovered the 3D distribution of an internal radioactive source, and the accuracy of the reconstructed result was confirmed by the micro-CT images. The *in vivo* CT imaging strategy is commonly used to validate artificial source-based optical experiments [13,14]. However, due to poor soft tissue contrast, it is difficult to determine the position of the tumor [14]. Cerenkov radiation based on radioactive molecular probes may help us solve this problem. The images of the subject labeled with a radioactive probe can be obtained both by nuclear imaging and optical imaging, which makes the nuclear imaging modality a useful validation tool. *In vivo* nuclear imaging modalities, including PET and SPECT, can obtain accurate functional information; if they are combined with the CT

modality, they can achieve 3D distribution of the molecular probes [27]. Therefore, they serve as an effective reference for optical imaging, especially for optical tomography.

In this study, we proposed a SPECT imaging validation strategy to verify the results of CLT. First, the same radioactive sources Na^{131}I utilized in the *in vitro* imaging experiment were implanted into adult athymic nude mice abdomens ($n = 6$). The activities of the sources were $100 \mu\text{Ci}$, $200 \mu\text{Ci}$, $300 \mu\text{Ci}$, $400 \mu\text{Ci}$, $500 \mu\text{Ci}$ and $600 \mu\text{Ci}$ respectively. The mice were then imaged by the aforementioned IVIS system with a 695-770 nm filter (Cy5.5). The luminescent images were acquired with a binning value of 4, integration time of 5 min and an aperture number $f_{\text{num}} = 1$. Next, the mice underwent SPECT imaging with the aforementioned SPECT-CT system for 20 min in the same supine position as for the optical acquisition, and images were reconstructed using a filtered back-projection algorithm. Using the previously described method, 3D distribution of an internal Na^{131}I radioactive source was reconstructed.

The reconstruction results both in localization and intensity of the $300 \mu\text{Ci}$ radioactive source are shown in Fig. 6. Figure 6(a) and Fig. 6(b) present the reconstruction results in horizontal, coronal, and sagittal views of CLT and SPECT imaging respectively. Comparison of the reconstruction results for all of the radioactive sources using CLT and SPECT imaging are listed in Table 2. The distance errors between the actual source, obtained from SPECT imaging, and the reconstructed one were acceptable. These data clearly showed the advantages of SPECT imaging validation for CLT and the potential to verify the results of optical molecular tomography. In addition, we further discussed the relationship between the radiotracer activity and the reconstructed maximum intensity. The maximum intensities of the reconstructed sources as a function of activity are depicted in Fig. 7. We found that the maximum intensity of the reconstructed source linearly increased with increasing activity. Moreover, there was a robust correlation between activity versus the maximum intensity ($r^2 = 0.966$). Our results suggested that localization and intensity of an embedded radioactive source with various concentrations could be recovered with certain accuracy.

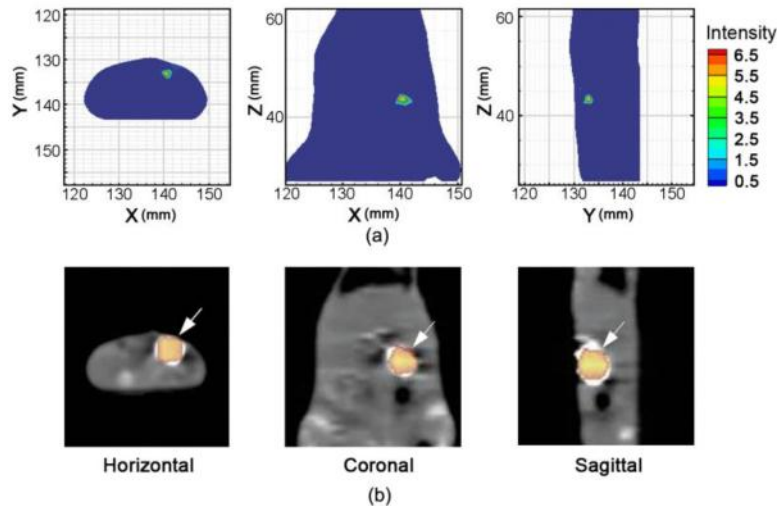


Fig. 6. The reconstruction results of the $300 \mu\text{Ci}$ Na^{131}I radioactive source. (a) and (b) are the reconstruction results in horizontal, coronal, and sagittal views of CLT and SPECT imaging respectively. Fusion of the reconstruction source with SPECT and CT images shows the exact SPECT reconstruction location of the implanted radioactive source (arrow). The images are shown in horizontal, coronal, and sagittal views.

Table 2. Comparison of reconstruction results obtained using CLT and SPECT

Radioactivity of source (μCi)	SPECT reconstructed location (mm)	CLT reconstructed location (mm)	d (mm)	CLT reconstructed maximum intensity
100	(76.82, 69.80, 31.50)	(76.43, 68.63, 32.17)	1.40	0.16
200	(100.90, 90.30, 28.00)	(102.32, 88.78, 27.94)	2.08	2.36
300	(140.00, 133.00, 43.00)	(140.10, 132.87, 43.42)	0.45	6.69
400	(102.87, 95.10, 32.00)	(101.80, 93.90, 33.50)	2.20	14.23
500	(96.11, 73.25, 29.00)	(96.49, 75.09, 30.46)	2.38	28.73
600	(87.44, 91.42, 26.00)	(88.11, 91.41, 26.46)	0.81	37.57

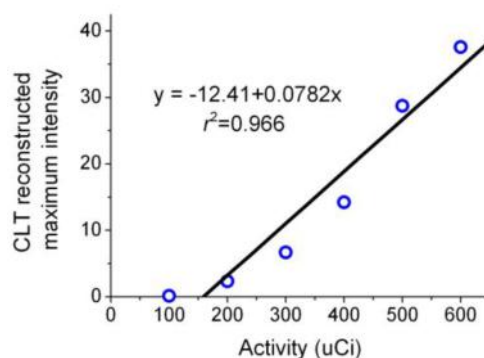


Fig. 7. Correlation analysis between CLT reconstructed maximum intensity and the radiotracer activity. There was a robust correlation between activity versus the maximum intensity ($r^2 = 0.966$).

4. Discussion and conclusions

Among the imaging modalities that can be used for noninvasive molecular imaging, optical imaging holds an important role in animal research because of its low cost, high sensitivity and molecular specificity [2,3]. We believe that research in optical imaging based on Cerenkov radiation will open new avenues for *in vivo* molecular imaging in small animals.

In vitro experiments showed that the radioactive sources emitted a mass of light and the measured spectrum presented a broad and continuous distribution from 500 nm to 900 nm, similar to previous studies [15,17,18]. Both of the results showed that the emitted light from Na^{131}I was correlated with Cerenkov radiation, and Cerenkov photon migration in tissues can be described by DE with acceptable accuracy. Moreover, *in vitro* experiments showed that there was a robust correlation between the optical signal versus the nuclear signal ($r^2 = 0.98$), thus Cerenkov luminescence imaging could reflect similar information as SPECT imaging.

In this study, we performed *in vivo* CLT based on a heterogeneous mouse model with an implanted Na^{131}I radioactive source. Li *et al.* presented CLT based on a homogeneous mouse model [19]. However, the assumption of a homogeneous optical property background will lead to inaccurate source reconstruction [22,26]. Our results showed that the reconstruction based on a heterogeneous mouse model was more accurate in localization than using the homogeneous one.

Moreover, a SPECT imaging validation strategy was also presented, in which SPECT imaging was regarded as a criterion. The distance errors between the actual source from SPECT imaging and the reconstructed one of CLT were acceptable. These data showed the strength of the SPECT imaging validation strategy for CLT, and its potential for verifying the results of optical tomography. In addition, localization and intensity of an embedded radioactive source with variable concentrations were recovered with certain accuracy, and a robust correlation between activity versus the reconstructed maximum intensity ($r^2 = 0.966$) was obtained.

Normally, optical imaging is used to detect visible or near-infrared light produced by fluorescent or bioluminescent probes. These imaging probes might hinder optical imaging application in clinics due to their potential toxicities. Radiotracers, such as [^{18}F]-FDG, Na^{18}F , and Na^{131}I , have been developed for PET or SPECT imaging, which have been widely used in clinics for the past several years. Cerenkov radiation based on radioactive probes relieves optical imaging from potential toxicities in traditional optical probes, opening new venues for preclinical research.

In conclusion, *in vivo* 3D CLT of small living animals demonstrated the ability of *in vivo* CLT to recover radioactive probe distribution in a heterogeneous mouse model. Moreover, this study showed the strength and benefit of the SPECT imaging validation strategy for CLT. Our future work will focus on the applications of this new imaging modality on tumor-bearing mice using radioactive probes.

Acknowledgements

We acknowledge Rongqing Zhang (Department of Cardiology, Xijing Hospital, Fourth Military Medical University), Runqiang Han, Kuan Peng, Nunu Ren, and Wei Li (Life Sciences Research Center, School of Life Sciences and Technology, Xidian University) during these experiments. This work is supported by the Program of the National Basic Research and Development Program of China (973) under Grant Nos. 2006CB705700, 2011CB707702, CAS Hundred Talents Program, the National Natural Science Foundation of China under Grant Nos. 81090272, 81000632, 30900334, the Shaanxi Provincial Natural Science Foundation Research Project under Grant No. 2009JQ8018, and the Fundamental Research Funds for the Central Universities.